Kinetics of Coarsening and Precipitation of Dilute Polymer Solutions: Fluorescence Study of PEO in Toluene

Susana Piçarra,[†] Eduardo J. N. Pereira,[‡] E. N. Bodunov,[†] and J. M. G. Martinho*[,†]

Centro de Química-Física Molecular, Instituto Superior Técnico, Av. Rovisco Pais, 1, 1049-001 Lisboa, Portugal; and Departamento de Física, Escola de Ciências, Universidade do Minho, 4700-057 Braga, Portugal

Received December 26, 2001; Revised Manuscript Received May 2, 2002

ABSTRACT: Fluorescence was used to follow the late stage phase demixing of a very dilute toluene solution of a poly(ethylene oxide) (PEO) chain labeled at one end with pyrene. The excimer to monomer fluorescence intensities ratio is proportional to the average volume of the aggregates. From the linear region of the fluorescence intensity ratio variation with time the apparent rate constants of coarsening were calculated. The apparent rates of coarsening increase with the temperature quench depth, owing to the decrease of the solvent quality to the polymer. At long times, large aggregates are formed and precipitate. From the variation of the light-scattering intensity the apparent rates of precipitation were calculated. A linear correlation was observed between the apparent rates of coarsening and precipitation.

1. Introduction

The spinodal phase demixing of binary fluid mixtures occurs in three stages: an early stage where loose aggregates are spontaneously formed, an intermediate stage where solvent is discharged until equilibrium concentrations in both the majority and minority phases are reached, and a final stage where aggregates grow by coarsening, to reduce their interfacial energy.[1−3] While the early stage is well understood, the intermediate stage is still very controversial. The late stage mechanism depends on the system components and composition.[4] For solutions with near-symmetrical compositions, an interconnected bicontinuous pattern is developed, while in very asymmetric systems polydisperse droplets coexist with a very dilute solution. The coarsening in bicontinuous pattern systems is driven by hydrodynamic effects,[5,6] while in asymmetric solutions it occurs either by the evaporation-condensation mechanism of Lifshitz−Slyozov−Wagner (LSW)[7,8] or by the diffusion−reaction mechanism of Binder−Sauffer (BS).[9,10] In the BS mechanism droplets travel by Brownian motion through the majority phase and coagulate when they meet. Contrarily, in the LSW mechanism, the translation motion of the droplets is negligible and larger droplets grow at the expense of the smaller ones in proximity: individual molecules leave small droplets, migrate through the majority phase by diffusion, and condensate into larger droplets. This results from the decrease of the chemical potential with droplet size increase due to surface tension. None of the BS and LSW mechanisms consider the particle−particle interactions and are restricted to systems with low volume fraction of the minority phase, $\Phi \ll {}^1/_{12}$.[11−13] The BS mechanism predominates when encounters between droplets are frequent. This depends on both the number density of droplets and the viscosity of the medium. For this reason the coarsening in dilute viscous systems (metal alloys and polymer blends) occurs by the LSW mechanism, but in dilute fluid solutions, it is the BS mechanism that predominates. Both mechanisms predict a linear increase of the average volume of droplets with time, with the slope being dependent on the volume fraction of the minority phase in the BS but not in the LSW mechanism.[13] The coarsening is responsible for the increase in droplets volume, reducing their number without changing the majority phase composition. When droplets larger than a critical volume are formed, precipitation in nonisopycnic systems occurs.[14,15]

The phase demixing of very dilute low molecular weight polymer solutions has been practically unexplored due to the low sensitivity of light-scattering and viscosimetry techniques commonly used. Here we take advantage of the high sensitivity of fluorescence to follow the coarsening of a 10^{-6} M PEO ($M_n = 4600$) solution in toluene, induced by temperature quenching. The PEO chain was labeled at one end with a pyrene derivative and the aggregation was followed by the formation of intermolecular excimer. It was shown that the excimer to monomer fluorescence intensities ratio I_E/I_M is proportional to the average volume of the aggregates. On the other hand, the integration of the coarsening kinetic rate equations showed that the initial growth of the particles average volume varies linearly with time. Combining both results, the apparent coarsening rate constants were calculated from the slopes of the plots of I_E/I_M with time. The rate constant increases with quench temperature depth owing to the increase of the efficiency of coagulation on the encounter. For sufficiently long times, I_E/I_M reaches a plateau due to the precipitation of large aggregates. In this stage, the scattered light intensity becomes proportional to the number density of aggregates and from their decrease in time the apparent precipitation rate constants were calculated. The precipitation and the coarsening rate constants at several temperatures are linearly correlated since the aggregates that precipitate are formed by coarsening.

2. Kinetics of Diffusion−Coalescence Coarsening

Droplets grow by a diffusion−reaction coarsening in the late stage of fluid dilute polymer solutions phase

* To whom correspondence should be addressed: E-mail: jgmartinho@ist.utl.pt. Telephone: 351 218419250.
[†] Instituto Superior Técnico.
[‡] Universidade do Minho.

10.1021/ma012235g CCC: $22.00
Published on Web 06/26/2002

demixing. This coarsening is identical to the Brownian coagulation of aerosols in rarefied gases.[16−18]

The time evolution of the number density of droplets, $n(v,t)$, of volume v at time t is given by the integro-differential equation[16]

$$\frac{\partial n(v,t)}{\partial t} = \frac{1}{2}\int_0^v k(u,v-u)n(u,t)n(v-u,t)\,\mathrm{d}u - n(v,t)\int_0^\infty k(v,u)n(u,t)\,\mathrm{d}u \quad (1)$$

where the first right-hand side term considers the formation of droplets of volume v by the encounter of two droplets of different sizes, while the second takes into account the disappearance of droplets of volume v by encounters with all droplets in solution. The factor of $^1/_2$ on the right-hand side of eq 1 prevents the double counting of collisions. The steady-state collision rate is given by the Smoluchowski equation[19,20]

$$k = 4\pi D(r_1 + r_2)p \quad (2)$$

where r_1 and r_2 are the radii of droplets 1 and 2, $D = D_1 + D_2$ is the mutual diffusion coefficient of the colliding particles, and p is the efficiency of coagulation on the droplets encounter. Introducing the diffusion coefficient $D_i = k_B T/6\pi\eta r_i$ for a particle or radius r_i, diffusing in a medium of viscosity η at temperature T, eq 2 rearranges to

$$k = \frac{k_e}{4}\frac{(v_1^{1/3} + v_2^{1/3})^2}{(v_1 v_2)^{1/3}} \quad (3)$$

where v_i is the volume of particle i and

$$k_e = \frac{8k_B T}{3\eta}p \quad (4)$$

is the collision rate for droplets of equal volumes. The integration over all particles gives

$$\frac{\mathrm{d}N(t)}{\mathrm{d}t} = \frac{1}{2}\int_0^\infty\int_0^v k(u,v-u)n(u,t)n(v-u,t)\,\mathrm{d}u\,\mathrm{d}v - \int_0^\infty\int_0^\infty k(u,v)n(u,t)n(v,t)\,\mathrm{d}u\,\mathrm{d}v \quad (5)$$

where

$$N(t) = \int_0^\infty n(v,t)\,\mathrm{d}v \quad (6)$$

is the total number density of droplets. Equation 5 can be further simplified since both integrals on the right-hand side are equal:

$$\frac{\mathrm{d}N(t)}{\mathrm{d}t} = -\frac{1}{2}\int_0^\infty\int_0^\infty k(v,u)n(v,t)n(u,t)\,\mathrm{d}u\,\mathrm{d}v \quad (7)$$

3. Numerical Calculations

To obtain the time evolution of the distribution of particles we proceed the numerical integration of eq 1, with the new adimensional variables

$$\Theta = N(0)k_e t \quad (8a)$$

$$X,Y = v/v_0 \quad (8b)$$

which allows one to rewrite eq 1 as

$$\frac{\partial n(X,\Theta)}{\partial\Theta} = \frac{1}{2}\int_0^X k_r(Y,X-Y)n(Y,\Theta)n(X-Y,\Theta)\,\mathrm{d}Y - n(X,\Theta)\int_0^\infty k_r(X,Y)n(Y,\Theta)\,\mathrm{d}Y \quad (9)$$

with $k_r = kv_0/k_e N(0)$.

The integration of eq 9 was performed considering an initial polydisperse distribution of particles described by a Gaussian centered at volume v_0 and with variance σ, which can be expressed in terms of adimensional variables, as

$$n(X,0) = \frac{1}{\sqrt{2\pi}\sigma_r}\exp\left\{-\frac{(X-1)^2}{2\sigma_r^2}\right\} \quad (10)$$

with $\sigma_r = \sigma/v_0$. The area of the distribution is unitary, which means that the total number density of particles at zero time is $N(0) = 1$. The integration was thus made in a fixed (sufficiently high) number of bins, linearly distributed between zero and the upper limit of integration, X_{cut}. The numerical algorithm used was the fifth-order Cash−Karp−Runge−Kutta algorithm with automatic adaptive step-size control for each individual integration step, which guaranties a good compromise between overall accuracy and accumulation of round off errors.[21] The method was developed for the so-called initial value problem of the integration of systems of ordinary differential equations, and several tests were made in order to ensure that the results were accurate enough and free from numerical artifacts. The number of bins for the size distributions was varied between 2000 and 8000, and the minimum fractional accuracy (for each time step integration and size bin) tested between 10^{-6} and 10^{-9}.

Figure 1 shows the results of the integration of eq 9 with the initial distribution given by eq 10, with reduced variance $\sigma_r = 0.25$ and superior limit of integration in the first integral equal to $X_{cut} = 50$. This means that the initial distribution is centered at v_0, has a variance of $0.25v_0$ and that particles with volumes larger than $50v_0$ are automatically removed from the calculations. These conditions describe a real system, where precipitation occurs when particles larger than a critical volume are generated.

The coarsening leads to the appearance of larger particles centered at nX_0 (with $n = 1, 2, \ldots$) and generate a pseudostationary distribution at very long times when particles larger than $X > X_{cut}$ precipitate.

Figure 2 shows the time evolution of the reciprocal of the number of particles (normalized to 1.0 at zero time), $N(0)/N(\Theta)$, generated from the initial distribution (eq 10) with reduced variance $\sigma_r = 0.20$.

The curves have an initial linear region whose duration depends on the cutoff volume of integration, X_{cut}, displaying an upward curvature for longer times. The linear region is described by

$$\frac{N(0)}{N(\Theta)} = 1 + 0.5\Theta \quad (11a)$$

and from eq 8a

$$\frac{N(0)}{N(t)} = 1 + 0.5N(0)k_e t = 1 + k_{co}t \quad (11b)$$

where $k_{co} = 0.5N(0)k_e$is taken as the coarsening rate constant. The numerical results show that eq 11a is

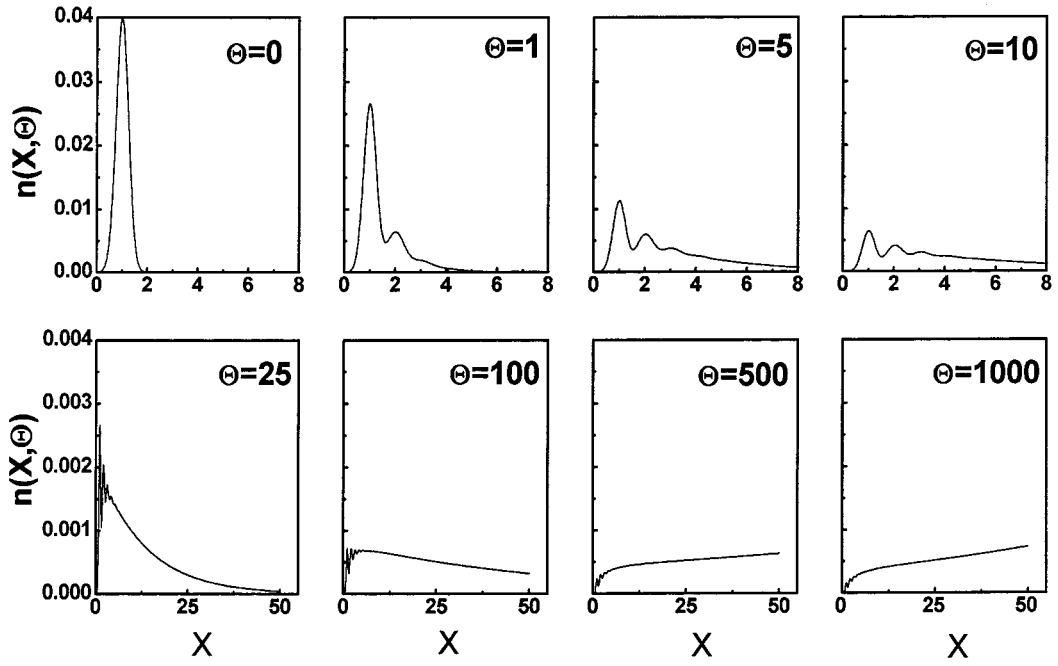

Figure 1. Plot of the number density of particles $n(X,\Theta)$ with the adimensional volume X, at several adimensional coarsening times, $\Theta = k_e N(0)t$, for an initial Gaussian distribution of particles size (eq 10) with reduced variance $\sigma_r = 0.25$.

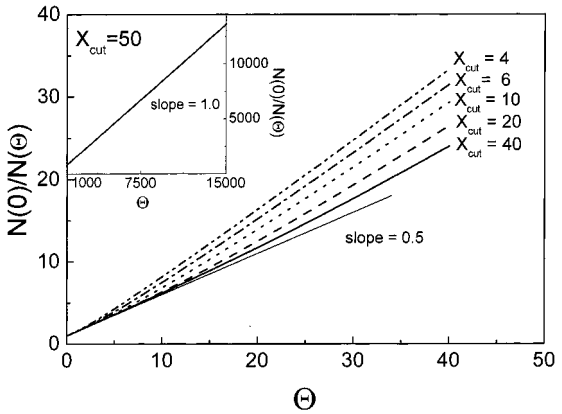

Figure 2. Variation of the ratio of the number density of particles at zero and Θ times, $\Theta = k_e N(0)t$, for an initial Gaussian distribution of particles size (eq 10) with reduced variance $\sigma_r = 0.20$, using several cutoff volumes, X_{cut}. Inset: $N(0)/N(\Theta)$ vs Θ for very long times and $X_{cut} = 50$.

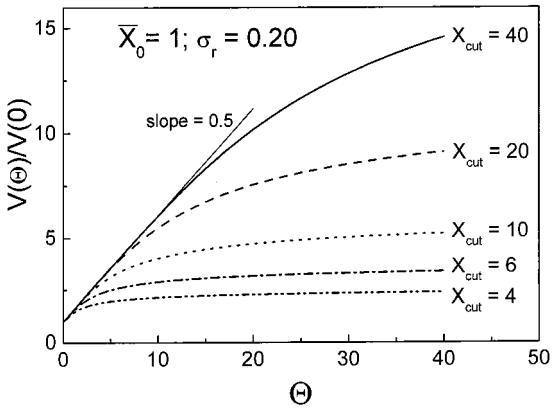

Figure 3. Variation of particles mean volume, $\bar{X} = \bar{V}/\bar{V}_0$, vs the adimensional time, $\Theta = k_e N(0)t$, for an initial Gaussian distribution of particles size (eq 10) with a reduced variance $\sigma_r = 0.20$, using several cutoff volumes, X_{cut}.

obeyed irrespective of the polydispersity of the system ($0 < \sigma_r < 0.25$). At longer times the curves show an upward curvature before reaching a new linear region with slope 1.0 (see inset in Figure 2). This slope is twice the value found at early times because at long times the collisions generate particles larger than X_{cut}, which are removed from the system by precipitation.

Figure 3 shows the time evolution of the average particles volume. All curves are linear at the initial times attaining a "plateau" at longer times, dependent on the superior limit of integration.

The plateau is a consequence of the development of a pseudostationary distribution of droplet sizes at long times (see Figure 1). These results suggest that when the superior limit of integration tends to infinite

$$\frac{\bar{V}(\Theta)}{\bar{V}(0)} = 1 + 0.5\Theta \qquad (12a)$$

and, from 8a

$$\frac{\bar{V}(t)}{\bar{V}(0)} = 1 + 0.5\ N(0)k_e t = 1 + k_{co}t \qquad (12b)$$

as found by Binder and Stauffer,[9,10] without considering the time evolution of the distribution of number density of particles. This slope is equal to the one obtained for the variation of $N(0)/N(t)$ vs t, since in the absence of precipitation the volume fraction of the minority phase, $\phi = N(t) \times \bar{V}(t)$, remains constant in time.

4. Experimental Section

Instrumentation. Fluorescence spectra were recorded on a SPEX Fluorolog F112A fluorometer at several temperatures using a cryostat from Oxford Instruments (DN 1704) that allows the control of the temperature within ±0.5 °C. The fluorescence spectra were recorded between 370 and 600 nm using 345 nm excitation light. The time evolution of the pyrene fluorescence was obtained in the SPEX Fluorolog, working in the time scan mode and using 345 nm excitation light with the emission wavelengths set at 376 nm (first pyrene monomer vibronic peak) and 480 nm (maximum of the pyrene excimer

Scheme 1

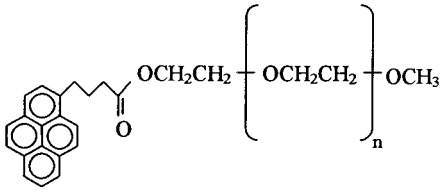

band). Molecular weight was determined by GPC with a Waters 510 HPLC pump, Waters U6K injector, Waters Ultrasyragel 10^3 Å column, and a Waters 2410 refractive index detector.

Light-scattering measurements were made in the same fluorometer with right angle geometry and using 360 nm light.

Polymer Synthesis and Materials. A poly(ethylene oxide) methyl ester chain with only one OH end group and molecular weight of ca. 5000 was purchased from Aldrich and purified by recrystallization in methanol. 4-(1-pyrenyl)butyric acid was obtained from Aldrich (97% purity) and used without further purification. Toluene (99.57%), from Riedel-de-Haën, was carefully dried over sodium during several days. Pyridine was dried over KOH before being fractionated. The synthesis procedure was described elsewhere.[22] Activated charcoal and silica gel were added at the end of the reaction in order to remove colored impurities and nonreacted 4-(1-pyrenyl)butyryl chloride.[23] The polymers were precipitated into cold methanol and further purified by gel permeation chromatography (GPC), using a Sephadex LH20 gel preparative column and methanol as eluent.[24] The structure of the polymer obtained (labeled at just one chain end) is represented in Scheme 1.

The polymer was characterized by GPC using PEO standards and THF as eluent. A molecular weight of $M_n = 4600$ ($M_w/M_n = 1.05$) was obtained.

Sample Preparation. A polymer solution with a concentration of 1.0×10^{-6} M was prepared in spectrograde toluene. The fluorescence cell with the solution was degassed by the freeze−pump−thaw technique (six cycles), the final pressure being lower than 10^{-5} bar. This cell was kept in the dark at +50 °C between measurements. Temperature quench measurements were made by introducing the cell inside the cryostat, already set to the desired temperature.

5. Results and Discussion

The fluorescence spectrum of a dilute (10^{-6} M) polymer solution in toluene, immediately after temperature quench, is composed of a unique structured band in the blue corresponding to the pyrene monomer emission. Intermolecular excimers are not formed since the solution is very dilute and the polymer chains do not have chance to encounter during the excited pyrene lifetime. For temperature quenches above 0 °C, the pyrene spectrum remains invariant in time for more than 30 h. Below this temperature, the excimer broad band centered at 480 nm appears and grows in time. This shows that the coexistence temperature for this polymer solution is around 0 °C.

Figure 4 shows the pyrene fluorescence spectra normalized at the peak of the first vibronic band, at several times after a temperature quench to −20 °C.

To obtain quantitative results during the initial times, the pyrene monomer ($\lambda_{em} = 376$ nm) and excimer ($\lambda_{em} = 480$ nm) fluorescence intensities were continuously recorded after introducing the cell at room temperature into a cryostat already set at −20 °C.

The monomer intensity initially increases, reaches a maximum, and then decreases to a plateau. The excimer intensity is zero before the monomer maximum, grows during monomer intensity decrease, and reaches a stationary value at the same time the monomer intensity attains the plateau. The initial pyrene monomer fluorescence intensity increase results from the decrease in the rate of the deactivation processes with temperature lowering. At this point, the excimer emission is negligible because polymer aggregation has not yet started. This time interval roughly coincides with the time necessary for temperature stabilization inside the fluorescence cell. After temperature stabilization, the excimer band appears and grows in time while the monomer intensity decreases. This shows that aggregation has started and that demixing occurs by instantaneous spinodal decomposition, without viscoelastic effects.[25] These effects, which retard the coarsening, are only expected for very long polymer chains where the presence of entanglements decreases collisions efficiency.[26,27] This is not the case for the present chain, since M_e (PEO) ∼ 5000.[28]

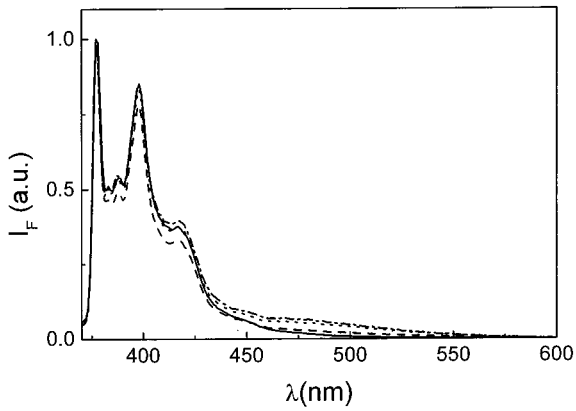

Figure 4. Fluorescence spectra of a 10^{-6} M solution of a pyrene-labeled PEO in toluene at several times after a temperature quench to −20 °C, with $\lambda_{exc} = 345$ nm: (—) immediately after the quench; (- - -) 5 min after the quench; (···) 10 min after the quench; (- · - · -) 1 h after the quench.

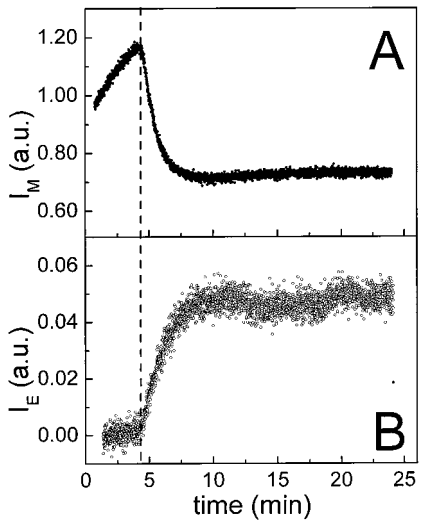

Figure 5. Variation of the monomer (A) ($\lambda_{exc} = 345$ nm and $\lambda_{em} = 376$ nm) and excimer (B) ($\lambda_{exc} = 345$ nm and $\lambda_{em} = 480$ nm) pyrene fluorescence intensities with time, immediately after a temperature quench to −20 °C.

Figure 6 shows the growth of the relative excimer to monomer fluorescence intensities, I_E/I_M, with time for several quench temperatures, after temperature stabilization.

The I_E/I_M ratios are linear with time, suggesting that a correlation should exist with the average volume of the particles (see Figure 3). In fact, according to the results presented in Appendix A (see eq A.13)

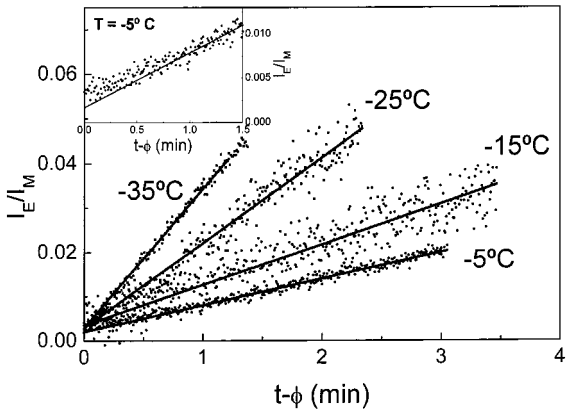

Figure 6. Pyrene excimer to monomer fluorescence intensities ratio, I_E/I_M, vs time after temperature stabilization, $t - \phi$, for several temperature quenches: −5, −15, −25, and −35 °C. Inset: Plot of initial time region of the I_E/I_M for a quench temperature of − 5 °C.

$$\frac{I_E}{I_M} = B\bar{V} \tag{13}$$

with

$$\bar{V} = \frac{1}{N}\sum_{i=i_0} n_i V_i \tag{14}$$

and B is a constant. From eqs 12 and 13, we obtain

$$\frac{I_E}{I_M} = \left(\frac{I_E}{I_M}\right)_0 + B\bar{V}_0 k_{co} t \tag{15}$$

with $\bar{V}_0$ being the particles average volume at $t = 0$ and $k_{co} = 0.5k_e N(0)$. Equation 15 only allows the calculation of an apparent rate constant (slope) since $B\bar{V}_0$ is unknown or difficult to estimate accurately. The increase of the slope of I_E/I_M with the decrease of the quench temperature (Figure 6) can be explained by both the variation of B and k_{co} with temperature. For low temperatures, the excimer dissociation is negligible ($k_{-1} \ll k_E$), and then (see eq A.14),

$$B = \frac{k_{fE}}{k_{fM}}\frac{k_1}{k_E}\frac{\rho N_{Av}}{M} \tag{16}$$

which means that B has the same dependence on temperature as k_1, since the ratio of the radiative rate constants, k_{fE}/k_{fM}, is temperature independent and k_E and ρ have a limited dependence on the temperature. As the excimer formation process between a pair of molecules is diffusion-controlled, B should increase with temperature. Then, the variation of the slope of I_E/I_M vs time with temperature has to be attributed to the variation of k_e. Lowering the temperature makes the solvent poorer for the polymer, leading to the formation of more compact globules and stronger intermolecular segment−segment interactions. Since the polymer molecular weight is below the critical entanglement molecular weight, viscoelastic effects are absent and permanent contacts between the colliding aggregates are favored (even if the globules are more compact), increasing the efficiency of coagulation (given by the p factor in eq 4). This effect dominates over the decrease of the diffusion coefficient of the aggregates resulting on the increase of the coarsening rate. Similar results were

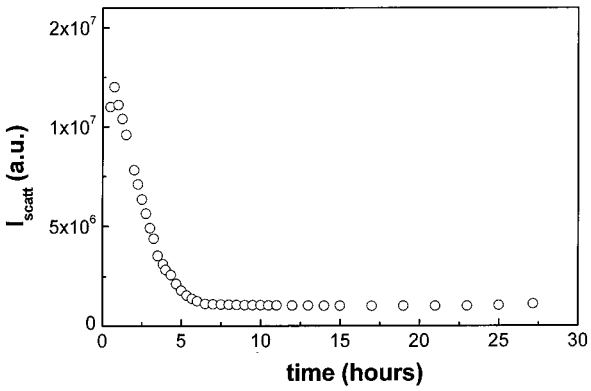

Figure 7. Plot of the scattered light intensity ($\lambda = 360$ nm) with time after a temperature quench to −20 °C for a scattering angle of 90°.

obtained for the phase demixing of concentrated polymer solutions,[29−31] which were explained by the increase of the thermodynamic driving force with temperature quench depth.

The plots in Figure 6 show a nonlinear initial region which is difficult to observe (see the inset for the quench temperature of − 5 °C). This corresponds to the fast initial and intermediate stages of phase demixing, which are difficult to study owing to their short duration and the uncertainty in the temperature stabilization time.

For longer times I_E/I_M reaches a plateau since both fluorescence intensities are stationary (see Figure 5). The plateau can be attributed either to precipitation (as demonstrated by numerical integration—see Figure 3) or to the formation of very large aggregates, where the excimer formation rate constants become independent of the aggregates size and given by eq 2. Precipitation is the most probable cause of the plateau since the system is nonisopycnic and precipitation occurs before large aggregates can be formed. Figure 7 shows the time evolution of the light-scattering intensity at a quench temperature of −20 °C, using 360 nm light and right angle geometry.

The scattering intensity increases initially due to the formation of large particles, decreases when precipitation removes the largest aggregates from the solution to reach a very low stationary value at long times. The scattering intensity for a monodisperse ensemble of N particles of molecular weight M and radius R, with light of intensity I_0 and wavelength in a vacuum, λ, is given by[32]

$$I_{scat}(t) = I_0 K N M^2 P(q,R,m) S(q) \tag{17}$$

where $P(q,R,m)$ is the intraparticle and $S(q)$ the interparticle scattering factors, $q = 4\pi n_{r0}/\lambda \sin(\theta/2)$ is the magnitude of the scattering vector at the scattering angle θ, $m = n_r/n_{r0}$ is the ratio between the refractive index of the medium and the solvents and K is an instrumental factor. For an ensemble of polydisperse scattering centers, the scattering intensity is

$$I_{scat}(t) = I_0 K \sum_i n_i M_i^2 P_i(q,R,m) S_i(q) \tag{18}$$

which can be written in the form

$$I_{scat}(t) = I_0 K N \sum_i \frac{n_i}{N} M_i^2 P_i(q,R,m) S_i(q) \tag{19}$$

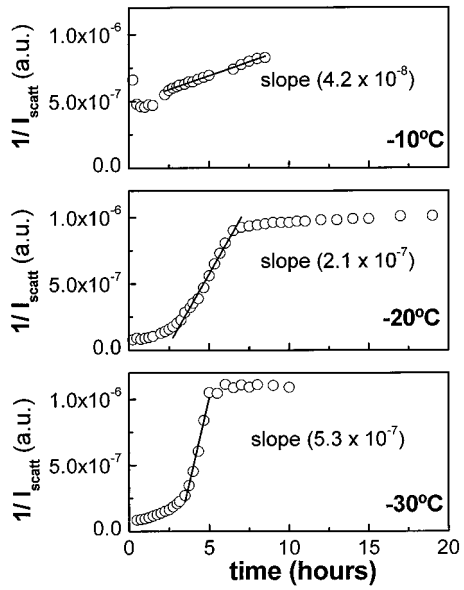

Figure 8. Plot of the reciprocal of the scattering intensity vs time for three temperature quenches: −10, −20, and −30 °C.

where n_i/N is the fraction of scattering centers of type i. In our case, and for long times, the sum in eq 19 becomes constant since (i) $S_i(q) = 1$ for dilute solutions, (ii) $P_i(q,R,m)$ is invariant (coarsening generates particles with self-similar shapes),[33] and (iii) $\sum n_i/N\, M_i^2$ is a constant because the system had reached the pseudo-stationary stage (shown by the numerical results of Figure 1). From this we can conclude that

$$I_{\text{scatt}} = CN(t) \tag{20}$$

where C is a constant that includes all the parameters in eq 19 except N. On the other hand, the numerical integration shows that for long times the reciprocal of the number density of particles with time changes linearly with time (see the inset in Figure 2), and therefore

$$\frac{N(0)}{N(t)} = 1 + N(0)k_e t \tag{21}$$

Introducing eq 20 in eq 21 gives

$$\frac{I_{\text{scatt},0}}{I_{\text{scatt}}} = 1 + N(0)\, k_e t = 1 + k_{pp} t \tag{22}$$

where $k_{pp} = 2k_{co}$ is the precipitation rate constant. Figure 8 shows the reciprocal of the scattering intensity with time for three temperature quenches.

The apparent precipitation rate constants (slopes of the linear region in the plots of Figure 8) increase with the temperature quench depth as observed for coarsening (see Figure 5) since both depend on k_e, which in turn decreases with temperature. Figure 9 confirms that the apparent rate constants are linearly correlated.

Unfortunately, since the apparent rate constants include parameters difficult to estimate accurately, it is not possible to confirm the two times factor predicted from numerical integration between the precipitation and coarsening rate constants.

6. Conclusions

The pyrene excimer to monomer fluorescence intensities ratio (I_E/I_M) was used to follow the coarsening process of a dilute solution of a one-end pyrene-labeled PEO chain in toluene. The coarsening occurs by a diffusion−reaction mechanism and from the integration of the kinetic rate equations it was found that the particles average volume increase linearly with time. On the other hand, it was shown that I_E/I_M is proportional to the average volume of the aggregates. Combining both results the coarsening apparent rate constant was calculated as the slope of the I_E/I_M plot with time. The rate constants increase with temperature quench depth due to the variation of the coagulation efficiency induced by the decrease of the quality of the solvent to the polymer.

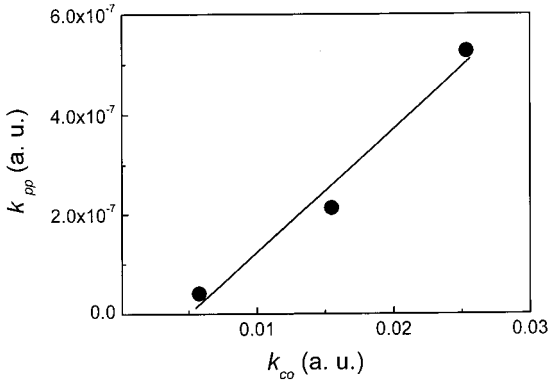

Figure 9. Variation of the apparent precipitation rate constant with the coarsening rate constant for three quench temperatures (−10, −20, and −30 °C).

Precipitation of droplets occurs at longer times since the system is nonisopycnic. In this time region, the decrease of the scattering intensity was used to calculate the apparent rate constant of precipitation. The apparent rates of coarsening and precipitation are linearly correlated because the precipitating droplets are formed by a coarsening process.

Fluorescence was proven to be an appropriate tool to study phase demixing. It allows the study of coarsening in very low molecular weight polymer solutions, which is difficult to follow by other techniques, especially for nonisopycnic systems.

Acknowledgment. The authors thank J. P. S. Farinha for critical reading the manuscript. This work was supported by the "Fundação para a Ciência e a Tecnologia" (FCT) under project POCTI/1999/QUI/33866. S.P. acknowledges the FCT for a Ph.D. grant (GGPXXI/BD/2979/96).

Appendix A. Monomer and Excimer Fluorescence Intensities for an Ensemble of Polydisperse Aggregates of One-End Pyrene-Labeled Chains

The monomer and the excimer fluorescence intensities of an ensemble of polydisperse aggregates of one-end pyrene-labeled chains in solution are given by

$$I_M = \sum_{i=0} f_i I_{Mi} \tag{A1}$$

$$I_E = \sum_{i=1} f_i I_{Ei} \tag{A2}$$

where f_i is the fraction of light absorbed by the aggregates with aggregation number i and I_{Mi} and I_{Ei} are the pyrene monomer and excimer fluorescence intensities of these aggregates, respectively. Assuming that

there are $(i - 1)$ pyrenes in the aggregate that can independently form excimers by collision with an electronic excited pyrene with rate constant k_1, according to the two-state Birks scheme[34]

$$I_{Mi} = I_0 q_M \frac{1}{1 + Fk_1(i-1)} \quad \text{(A3)}$$

$$I_{Ei} = I_0 q_E \frac{Fk_1(i-1)}{1 + Fk_1(i-1)} \quad \text{(A4)}$$

where q_M and q_E are the quantum yields of the pyrene monomer and excimer, respectively, and

$$F = \frac{k_E}{k_M(k_E + k_{-1})} \quad \text{(A5)}$$

where k_M, k_E are the intrinsic rate constants of deactivation of the pyrene monomer and excimer, respectively, and k_{-1} is the excimer dissociation rate constant. The fraction of light absorbed by the aggregates, in a very low concentration, with aggregation number i, is given by

$$f_i = 2.303\epsilon i n_i l \quad \text{(A6)}$$

where ϵ is the absorption coefficient of pyrene at the excitation wavelength, n_i is the number density of the aggregates, and l is the optical path of the excitation light within the medium. From eqs A.1, A.2, A.3, A.4, and A.6

$$I_M = I_0 \times 2.303\epsilon l q_M \left[n_1 + \sum_{i=2} \frac{n_i i}{1 + Fk_1(i-1)} \right] \quad \text{(A7)}$$

$$I_E = I_0 \times 2.303\epsilon l q_E \times \sum_{i=2} \frac{Fk_1(i-1)n_i i}{1 + Fk_1(i-1)} \quad \text{(A8)}$$

According to the phase diagram, the polymer concentration in the majority phase is almost negligible and $n_1 \approx 0$. Since for pyrene at room temperature, $k_M \sim 4 \times 10^6$ s^{-1}, $k_E \sim 2 \times 10^7$ s^{-1}, $k_{-1} \sim 2 \times 10^6$ s^{-1},[34] and $k_1 \sim 10^7$ s^{-1} (estimated from pyrene excimer kinetics in micelles [35,36]) it is reasonable to consider that $Fk_1 > 1$. Then, after the initial and the intermediate stages, when coarsening starts ($i > i_0$), $Fk_1 i_0 \gg 1$ and

$$I_M = I_0 \times 2.303\epsilon l q_M \sum_{i=i_0} \frac{n_i}{Fk_1} = \frac{I_0 \times 2.303\epsilon l q_M}{Fk_1} N \quad \text{(A9)}$$

$$I_E = I_0 \times 2.303\epsilon l q_E \times \sum_{i=i_0} n_i i \quad \text{(A10)}$$

The ratio of eqs A.10 and A.9 gives

$$\frac{I_E}{I_M} = \frac{q_E}{q_M} Fk_1 \sum_{i=i_0} \frac{n_i i}{N} \quad \text{(A11)}$$

where $N = \sum_{i=1} n_i$ is the total number of aggregates in solution. The aggregation number is, on the other hand, proportional to its volume, as soon as the particle density, ρ, is invariant with size

$$i = \frac{V_i \rho N_{Av}}{M} \quad \text{(A12)}$$

where M is the molecular weight of the polymer chain and N_{Av} is Avogadro's number. Introducing eq A.12 into eq A.11

$$\frac{I_E}{I_M} = \frac{q_E}{q_M} Fk_1 \frac{\rho N_{Av}}{M} \sum_{i=i_0} \frac{n_i}{N} V_i = B\bar{V} \quad \text{(A13)}$$

where B

$$B = \frac{k_{fE}}{k_{fM}} \frac{k_1}{(k_E + k_{-1})} \frac{\rho N_{Av}}{M} \quad \text{(A14)}$$

is a constant.

References and Notes

(1) Gunton, J. D.; San Miguel, M.; Sahni, P. In *Phase Separation and Critical Phenomena*; Domb, C., Lebowitz, J. H., Eds.; Academic: London, 1983; Vol. 8.
(2) Furukawa, H. *Adv. Phys.* **1985**, *34*, 703.
(3) Hashimoto, T. *Phase Transitions* **1988**, *12*, 47.
(4) Tanaka, H. *J. Chem. Phys.* **1994**, *100*, 5323.
(5) Siggia, E. D. *Phys. Rev. A* **1979**, *20*, 595.
(6) Tanaka, H. *Phys. Rev. E* **1995**, *51*, 1313.
(7) Lifshitz, I. M.; Slyozov, V. V. *J. Phys. Chem. Solids* **1961**, *19*, 35.
(8) Wagner, C. *Z. Electrochem.* **1961**, *65*, 581.
(9) Binder, K.; Stauffer, D. *Phys. Rev. Lett.* **1974**, *33*, 1006.
(10) Binder, K.; Stauffer, D. *Adv. Phys.* **1976**, *25*, 343.
(11) San Miguel, M.; Grant, M.; Gunton, J. D. *Phys. Rev. A* **1985**, *31*, 1001.
(12) Tanaka. H. *Phys. Rev. Lett.* **1994**, *72*, 1702.
(13) Tanaka, H. *J. Chem. Phys.* **1995**, *103*, 2361.
(14) Philip, J. R.; Smiles, D. E. *Adv. Colloid Interface Sci.* **1982**, *17*, 83.
(15) Hunter, R. J. *Foundations of Colloid Science*; Oxford Science Pub.: Oxford, England, 1987; Vol. I.
(16) Wagner, P. E.; Kerker, M. *J. Chem. Phys.* **1977**, *66*, 638.
(17) Davies, C. N. *J. Aerosol Sci.* **1979**, *10*, 151.
(18) Wagner, P. E.; Kerker, M. *J. Colloid Interface Sci.* **1980**, *73*, 244.
(19) Smoluchowski, M. *Z. Phys. Chem.* **1917**, *92*, 129.
(20) Collins, F. C.; Kimball, G. E. *J. Colloid Sci.* **1949**, *4*, 425.
(21) Press, W. H.; Teukolsky, S. A.; Vetterling, W. T.; Flannery, B. P. *Numerical Recipes in Fortran, The Art of Scientific Computation*, 2nd. ed.; Cambridge University Press: Cambridge, England, 1992.
(22) Cheung, S.-T.; Winnik, M. A.; Redpath, E. C. *Makromol. Chem.* **1982**, *183*, 1815.
(23) Winnik, M. A.; Redpath, A. E. C.; Paton, K.; Danhelka, J. *Polymer* **1984**, *1251*, 91.
(24) Ghiggino, K. P.; Snare, M. J.; Thistlethwaite, P. J. *Eur. Polym. J.* **1985**, *21*, 265.
(25) Piçarra, S.; Martinho, J. M. G. *Macromolecules* **2001**, *34*, 53.
(26) Tanaka, H. *Macromolecules* **1992**, *25*, 6377.
(27) Tanaka, H. *J. Chem. Phys.* **1994**, *100*, 5323; *Phys. Rev. Lett.* **1993**, *71*, 3158.
(28) Wool, R. P. *Polymer Interfaces, Structure and Strength*; Hanser Publishers: New York, 1993.
(29) Graham, P. D.; McHugh, A. J. *Macromolecules* **1998**, *31*, 2565.
(30) Song, S.-W.; Torkelson, J. M. *Macromolecules* **1994**, *27*, 6389.
(31) Song, S.-W.; Torkelson, J. M. *Macromolecules* **1995**, *28*, 209.
(32) Hallett, F. R. In *Light Scattering, Principles and Development*; Brown, W., Ed.; Oxford Science Publications: Oxford, England, 1996.
(33) Kubota, K.; Kuwahara, N. *Phys. Rev. Lett.* **1992**, *68*, 197.
(34) Birks, J. B *Photophysics of Aromatic Molecules*; Wiley-Interscience, New York, 1970.
(35) Atik, S. S.; Nam, M.; Singer, L. A. *Chem. Phys. Lett.* **1979**, *67*, 75.
(36) Malliaris, A.; Le Moigne, J.; Sturm, J.; Zana, R. *J. Phys. Chem.* **1985**, *89*, 2709.

MA012235G